A Numerical Study of the Kinetic Origins of Two-Stage Autoignition and the Dependence of Autoignition Temperature on Reactant Pressure in Lean Alkane-Air Mixtures

F. Battin-Leclerc[1], F. Buda[1], M. Fairweather*[2], P.A. Glaude[1], J.F. Griffiths[3], K.J. Hughes[3], R. Porter[2] and A.S. Tomlin[2]

[1]Umr 7630 CNRS, DCPR, Département De Chimie Physique des Réactions ENSIC-INPL, 1, rue Grandville, BP 451, 54001 NANCY Cedex, France

[2]School of Process, Environmental and Materials Engineering, University of Leeds, Leeds LS2 9JT, UK

[3]School of Chemistry, University of Leeds, Leeds LS2 9JT, UK

Abstract

In this work we investigate by numerical methods, the autoignition temperature of lean mixtures of n-butane in air, and show how it varies within a range of temperatures and compositions. We show that relatively small increases of pressure above atmospheric, of even rather lean mixtures, can autoignite at 550 K. The primary results are evaluated with respect to published experimental studies. The kinetic foundation is then analysed by formal numerical methods to trace the origins of the dramatic shifts in autoignition temperatures as conditions are changed. The most important reactions leading to hydrogen peroxide formation are identified using rate of production analysis, and the greatest heat releasing reactions are determined in the transition from cool flame to ignition.

Introduction

The usual sources of data on "autoignition temperatures of organic gases or vapours" (AIT) refer to the minimum temperature at which spontaneous ignition takes place in a particular vessel (e.g. BS 4056 and IEC standard 79-4 (1975), or ASTM-E 659-78), in a mixture with air at atmospheric pressure [1]. The AIT's of normal alkanes, e.g. C_3H_8 to n-C_9H_{20}, show a dramatic decrease from C_3H_8, at 790 K, through n-C_4H_{10} and n-C_5H_{12}, at 700 and 560 K respectively, to n-C_9H_{20} at 510 K. However, the autoignition temperature for a given reactant will not be the same under different conditions, such as varying vessel size or, more importantly in the present context, reactant pressure or composition. It follows that there are potential hazards in industrial processing over wide ranges of conditions involving temperatures that are otherwise deemed to be safe according to statutory autoignition test procedures.

One of the key factors in the chemistry that promotes autoignition at low temperatures (T < 700 K) is the transition from a cool flame to a second stage, within a two-stage ignition. The development of the second stage is believed to be driven by the formation and decomposition of hydrogen peroxide [2-6].

The kinetic significance of H_2O_2 lies in the chain branching step,

$$H_2O_2 + M \rightarrow 2OH + M. \quad (1)$$

This becomes important at temperatures in the approximate range 800 – 1000 K, where chain propagation by HO_2 radicals tends to predominate. Unless reaction pressures are unusually low, the reaction,

$$H + O_2 \rightarrow OH + O \quad (2)$$

does not play a major part in chain branching until the temperature is beyond 1000 K [7].

Our interest is to investigate quantitatively the kinetic origins of hydrogen peroxide in the transition stage. In this paper we use comprehensive models to simulate the combustion of lean n-butane in air. One of the models is then reduced by formal methods in order to generate a reaction scheme of sufficient simplicity and generality that it may be incorporated in predictive tools for combustion hazards (as part of the EU "Safekinex" project, EVG1-CT-2002-00072). There is some relevance also to the development of fuels for use in HCCI combustion, where autoignition of fuel lean mixtures occurs with chemical kinetics playing a greater role than in other types of engine. For the present purpose we analyse the behaviour at an intermediate stage of reduction. The most important sequences of reactions leading to H_2O_2 formation are identified and the mechanistic implications are discussed.

Numerical Models and Methods

There is currently a great interest in reduced kinetic models to represent hydrocarbon combustion, including their coupling to flow dynamics in complex three-dimensional reactive flows for the application of explosion prevention computer tools in hydrocarbon oxidation processes. To be valid, such models must be capable of reproducing the various autoignition phenomena seen in experiments over a wide range of operating conditions.

*Corresponding author: m.fairweather@leeds.ac.uk

In this study we examine the dependence of the ignition limits on fuel/air composition above atmospheric pressure and the principal kinetic interactions leading to hydrogen peroxide formation during two-stage ignition using a reduced kinetic model for n-butane oxidation. In this work the intention was not to produce an optimal reduced mechanism but to provide a scheme that was small enough to allow further kinetic investigation. The reduced model was developed from a comprehensive mechanism that was derived at CNRS-DCPR, Nancy using EXGAS software [8]. The comprehensive mechanism comprises 128 species in 313 irreversible reactions and 417 reversible reactions and has generalized kinetic features taking the simplified form shown in fig. 1. The overall structure is described in detail elsewhere [9].

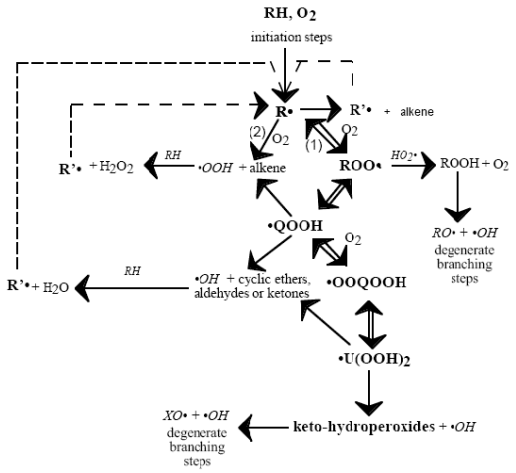

Fig. 1 Simplified scheme for the primary mechanism of the oxidation of alkanes (broken lines represent metathesis with the initial alkane RH) [9].

For comparison, a second comprehensive model for n-butane oxidation was tested which was derived from the C7 model developed by Westbrook et al [10].

The numerical calculations were carried out for the zero-dimensional model described below using the SPRINT integration package [11]. SPRINT solves the coupled differential equations describing the rate of change of concentration of each chemical species and energy conservation: in a closed vessel. The rate of change of concentration is given by:

$$\frac{d[c_i]}{dt} = \sum_j v_{ij} R_j \quad , \tag{3}$$

where c_i is the concentration of species i, v_{ij} is the stoichiometric coefficient of the species i in the reaction j and R_j is the *jth* reaction rate. Energy conservation is described by:

$$(Cv)\frac{dT}{dt} = \sum_j \Delta H_j^o R_j - \frac{UA}{V}(T - T_a), \tag{4}$$

where Cv is heat capacity, ΔH_j is the enthalpy of reaction j, V the volume, A the reactor surface area, U the heat transfer coefficient and T_a is the ambient temperature. The heat loss rate was calculated on the basis of Newtonian cooling through the walls. Predictions of the full scheme were evaluated by constructing $\varphi - T_a$ ignition diagrams over the fuel lean range and comparing with experimental data [1].

The reduced mechanism was developed by first identifying necessary species based on the analysis of the system Jacobian [12]. The necessary species include selected important species as defined by the user, and other species for which realistic concentrations are required in order to reproduce the concentrations of important species or important reaction features. The sensitivity of the rate of production of an N-membered group of important species to a change in concentration of species i, is given by:

$$B_i = \sum_{n=1}^{N} \left(\partial \ln f_n / \partial \ln c_i\right)^2 , \tag{5}$$

where f_n is the rate of production of species n. The higher the B_i value the greater the direct effect of species i on the rate of production of important species. Necessary species with indirect effects on the important species are taken into account by an iterative procedure, whereby the B_i values are calculated for all species and the species with the highest B_i value is incorporated into the N-membered group after each calculation. The procedure is repeated again and again until vector **B** converges and a large gap appears between the ranked B_i values of necessary and redundant species as they form definite groups. Equation (5) was applied using KINALC subroutines [13, 14]. The union of identified necessary species was taken at selected time points during the simulations under which the reduction was performed and then the process was repeated until an intermediate reduced scheme with 58 species in 277 reactions was created.

In order to investigate the kinetic properties that lead to runaway reaction, a two-stage ignition was simulated at a specific operating condition. Selected time points in the transition from cool flame to full ignition were further analyzed using rate of production analysis and calculated heat release rates. The effect of temperature on important kinetic processes involving hydrogen peroxide was then examined.

Results and Discussion

First we present a comparison of predictions from the full schemes with experimental data. Figures 2 and 3 show the simulated $\varphi - T_a$ ignition diagrams for n-butane and air for the Nancy and Westbrook schemes respectively. The condition of analysis of 600K and 1.64% n-C_4H_{10} for the Nancy scheme is marked on Fig. 2 by an arrow. The qualitative features of the experimental $\varphi - T_a$ ignition boundary [1], shown in Fig. 4, are captured by the numerical models showing both

cool flame and two stage ignition behaviour. The reverse "s" shape of the boundary is displayed by both the models and this is an important validation. However Fig. 5 shows that at lower concentrations of fuel there are quantitative disagreements with the experiment, and both models over-predict the autoignition temperatures. This may imply a shortcoming in the way that the intermediate molecular products that lead to high-temperature reactions are interpreted [15]. There may also be some discrepancy due to inhomegeneities of temperature in the unstirred vessel [1]. At higher concentrations of fuel the Nancy model shows very good agreement with the experiment but the autoignition temperatures in this region are under predicted by the Westbrook model.

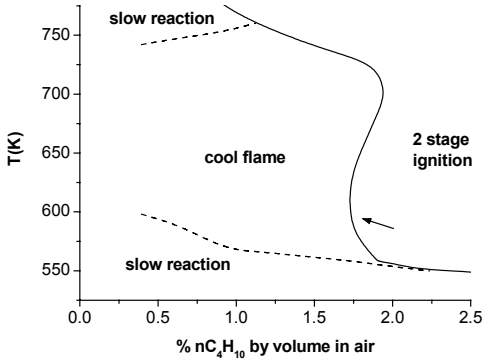

Fig. 2 Nancy scheme simulated φ – T_a ignition diagram for lean n-C_4H_{10} + air in a closed vessel under spatially uniform conditions.

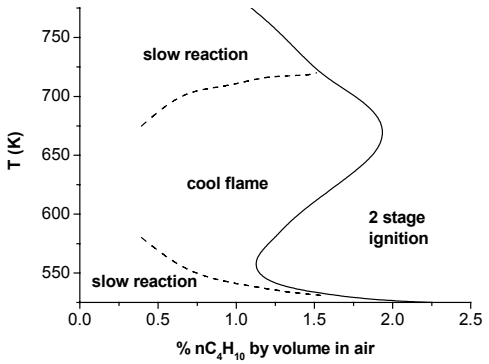

Fig. 3 Westbrook *et al* scheme simulated φ – T_a ignition diagram for lean n-C_4H_{10} + air in a closed vessel under spatially uniform conditions.

The comparison of the experimental ignition boundaries at 0.1 MPa and 0.2 MPa shown in Fig. 4 gives an insight into the potential hazards in industrial processing. In fact, the lowest temperature for autoignition of n-butane (the AIT) falls markedly when there is a small increase in pressure to above *ca*. 0.15 MPa. This reinforces the need for hazard prediction tools.

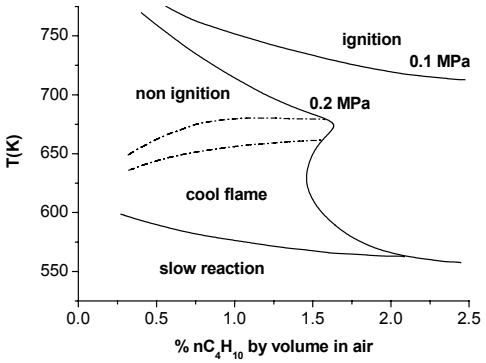

Fig. 4 φ – T_a ignition diagram for n-C_4H_{10} + air at 0.2 MPa and 0.1 MPa (ignition boundary only) in an unstirred stainless steel reaction vessel (0.5 dm^3) [1].

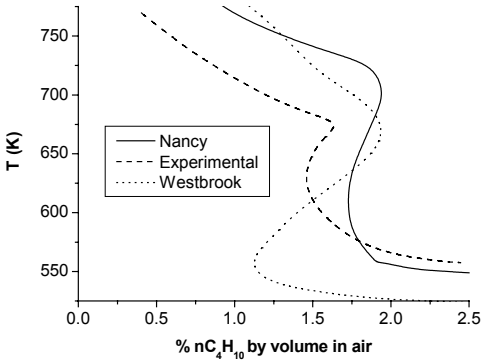

Fig. 5 Comparison of experimental and numerically predicted full scheme φ – T_a diagrams (closed vessel 0.2 MPa).

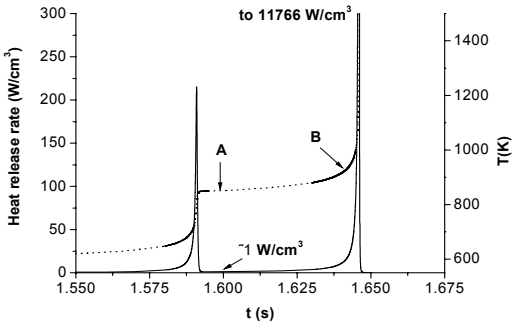

Fig. 6 Heat release rate during two-stage ignition (1.64 % n-C_4H_{10} in air at 0.2 MPa and 600 K). Points A (t=1.6 s, T=851 K) and B (t=1.64 s, T=916 K) were investigated kinetically.

Fig. 6 shows the net heat release rate and temperature as functions of time from the initial conditions of 600K and 1.64% n-C_4H_{10}. The temperature stabilizes after the cool flame with a small net heat release of 1 W/cm^3. The maximum heat release during the cool flame is 215

Formation reactions	A%	B%	Removal reactions	A%	B%
H_2O_2					
$HO_2 + HO_2 \leftrightarrow H_2O_2 + O_2$	49.7	71.6	H_2O_2 (+M) $\rightarrow$ 2OH (+M)	70.4	69.8
$CH_3CHO + HO_2 \leftrightarrow CH_3CO + H_2O_2$	24.4	11.7	$H_2O_2 + OH \leftrightarrow H_2O + HO_2$	18.0	23.8
$HO_2 + CH_2O \leftrightarrow CHO + H_2O_2$	23.0	14.3	$CH_3O_2 + H_2O_2 \leftrightarrow CH_3O_2H + HO_2$	6.5	1.2
$C_2H_5CHO + HO_2 \rightarrow C_2H_5CO + H_2O_2$	1.1	1.1	$H_2O_2 + H \leftrightarrow H_2O + OH$	4.3	4.5
[a] n-$C_4H_{10} + HO_2 \rightarrow C_4H_9 + H_2O_2$	1.3	-			
$C_4H_8 + HO_2 \rightarrow C_4H_7 + H_2O_2$	0.5	-			
CH_2O					
CH_3O (+M) $\leftrightarrow CH_2O + H$ (+M)	67.2	59.8	$CH_2O + OH \leftrightarrow CHO + H_2O$	71.8	82.0
$O_2 + C_2H_3 \leftrightarrow CH_2O + CHO$	11.7	18.7	$CH_2O + HO_2 \leftrightarrow CHO + H_2O_2$	17.4	8.2
$C_3H_7CO_3H \rightarrow OH + CH_2O + CO + C_2H_4$	6.3	-	$CH_2O + H \leftrightarrow CHO + H_2$	8.9	8.3
$C_2H_4 + OH \leftrightarrow CH_3 + CH_2O$	4.5	7.8	$CH_3O_2 + CH_2O \leftrightarrow CH_3O_2H + CHO$	0.9	-
$C_4H_8 + OH \rightarrow CH_2O + C_2H_4 + CH_3$	3.1	3.8	$CH_2O + O \leftrightarrow CHO + OH$	-	1.2
$O_2 + CH_3O \leftrightarrow CH_2O + HO_2$	3.0	1.4			
$C_2H_5 + HO_2 \rightarrow CH_3 + CH_2O + OH$	1.4	2.7			
$C_3H_5O_2H \rightarrow C_2H_3 + CH_2O + OH$	-	2.6			
HO_2					
$O_2 + CHO \leftrightarrow CO + HO_2$	61.4	64.9	$HO_2 + HO_2 \leftrightarrow H_2O_2 + O_2$	42.8	47.5
$C_2H_5 + O_2 \leftrightarrow C_2H_4 + HO_2$	10.7	10.2	$CH_3 + HO_2 \leftrightarrow CH_3O + OH$	24.5	26.3
$H + O_2$ (+M) $\leftrightarrow HO_2$ (+M)	9.6	8.4	$CH_3CHO + HO_2 \leftrightarrow CH_3CO + H_2O_2$	10.5	3.9
[a] $C_4H_9 + O_2 \rightarrow C_4H_8 + HO_2$	8.1	4.7	$CH_2O + HO_2 \leftrightarrow CHO + H_2O_2$	9.9	4.8
$H_2O_2 + OH \leftrightarrow H_2O + HO_2$	4.1	8.2	$C_4H_7 + HO_2 \rightarrow C_4H_7O_2H$	3.7	5.0
$CH_3O_2 + H_2O_2 \leftrightarrow CH_3O_2H + HO_2$	1.5	-	$CO + HO_2 \leftrightarrow CO_2 + OH$	2.1	3.1
$C_4H_8O_2H \rightarrow C_4H_8 + HO_2$	1.4	0.8	$CH_3O_2 + HO_2 \leftrightarrow CH_3O_2H + O_2$	1.7	-
$CH_3O + O_2 \leftrightarrow CH_2O + HO_2$	1.3	-	$HO_2 + H \leftrightarrow OH + OH$	1.0	2.6
$H + O_2$ ($+H_2O$) $\leftrightarrow HO_2$ ($+H_2O$)	1.2	1.3	$HO_2 + OH \leftrightarrow H_2O + O_2$	-	1.8
			$C_2H_5 + HO_2 \rightarrow CH_3 + CH_2O + OH$	-	1.2
			$C_3H_5 + HO_2 \rightarrow C_3H_5O_2H$	-	1.2
CHO					
$CH_2O + OH \leftrightarrow CHO + H_2O$	65.8	71.1	$O_2 + CHO \leftrightarrow CO + HO_2$	98.9	97.7
$CH_2O + HO_2 \leftrightarrow CHO + H_2O_2$	15.9	7.1	CHO (+M) $\leftrightarrow$ H + CO (+M)	-	2.1
$CH_2O + H \leftrightarrow CHO + H_2$	8.2	7.2			
$C_2H_3 + O_2 \leftrightarrow CH_2O + CHO$	8.2	12.8			
$CH_2O + O \rightarrow CHO + OH$	-	1.0			

[a] isomers combined

Table 1: Rates of production and removal, expressed as % contribution, for reaction in a closed vessel reactions in a closed vessel related to points A and B in Fig. 7.

Heat output rates / W cm $^{-3}$		Heat consumption rates / W cm $^{-3}$	
$O_2 + CHO \leftrightarrow CO + HO_2$	0.48	H_2O_2 (+M) $\leftrightarrow$ 2OH (+M)	0.20
$CH_2O + OH \leftrightarrow CHO + H_2O$	0.3	CH_3O (+ M) $\leftrightarrow CH_2O + H$ (+ M)	0.15
$2HO_2 \leftrightarrow H_2O_2 + O_2$	0.19	$CO + CH_3$ (+M) $\leftrightarrow CH_3CO$ (+M)	0.058
$HO_2 + CH_3 \leftrightarrow CH_3O + OH$	0.14	$C_4H_7O_2H \leftrightarrow OH + CH_3CHO + C_2H_3$	0.056
$O_2 + H$ (+M) $\leftrightarrow HO_2$ (+M)	0.12	$CH_3O_2H \leftrightarrow CH_3O + OH$	0.043
$O_2 + C_2H_3 \leftrightarrow CH_2O + CHO$	0.11	$C_4H_9 \rightarrow CH_3 + C_3H_6$	0.018
[a] $C_4H_{10} + OH \rightarrow H_2O + C_4H_9$	0.082	$C_4H_9O_2 \leftrightarrow C_4H_8O_2H$	0.013
$C_4H_8 + OH \rightarrow C_4H_7 + H_2O$	0.062	$C_4H_9 \rightarrow C_2H_5 + C_2H_4$	0.011
$O_2 + CH_3$ (+M) $\leftrightarrow CH_3O_2$ (+M)	0.043	$C_4H_8O_4H \rightarrow OH + C_3H_7CO_3H$	0.008
$CH_3CHO + OH \leftrightarrow CH_3CO + H_2O$	0.041	$C_3H_5O_2H \rightarrow OH + CH_2O + C_2H_3$	0.006

[a] isomers combined

Table 2: Individual heat output / consumption rates in the post cool flame region at point A in Fig. 7.

Heat output rates / W cm $^{-3}$		Heat consumption rates / W cm $^{-3}$	
$O_2 + CHO \leftrightarrow CO + HO_2$	3.5	H_2O_2 (+M) $\leftrightarrow$ 2OH (+M)	2.1
$CH_2O + OH \leftrightarrow CHO + H_2O$	2.4	CH_3O (+ M) $\leftrightarrow$ CH_2O + H (+ M)	1.0
$2HO_2 \leftrightarrow H_2O_2 + O_2$	1.5	$C_4H_7O_2H \leftrightarrow OH + CH_3CHO + C_2H_3$	0.53
$O_2 + C_2H_3 \leftrightarrow CH_2O + CHO$	1.3	$CO + CH_3$ (+M) $\leftrightarrow$ CH_3CO (+M)	0.25
$HO_2 + CH_3 \leftrightarrow CH_3O$+ OH	1.1	$C_4H_9 \rightarrow C_2H_5 + C_2H_4$	0.15
$O_2 + H$ (+M) $\leftrightarrow$ HO_2 (+M)	0.71	$C_4H_9 \rightarrow CH_3 + C_3H_6$	0.15
C_4H_8+ OH $\rightarrow$ $C_4H_7 + H_2O$	0.64	$C_3H_5O_2H \rightarrow OH + CH_2O + C_2H_3$	0.15
$H_2O_2 + OH \leftrightarrow H_2O + HO_2$	0.45	$CH_3O_2H \leftrightarrow CH_3O + OH$	0.077
$HO_2 + CO \leftrightarrow CO_2 + OH$	0.31	CHO (+ M) $\leftrightarrow$ H + CO (+ M)	0.043
C_2H_5 (+M) $\leftrightarrow$ C_2H_4 + H (+M)	0.31	$O_2 + H \leftrightarrow OH + O$	0.041

Table 3: Individual heat output / consumption rates in the post cool flame region at point B in Fig. 7.

W/cm^3 and in the final stage of ignition the highest predicted rate of heat release is ~11.8 kW/cm^3. The rate of temperature rise is at its highest when these maxima occur. The very low heat release rate after the cool flame is symptomatic of the suppression of activity caused by the negative temperature coefficient (ntc) of overall reaction rate [16]. Selected points for kinetic studies in the transition from cool flame to ignition are marked by arrows. Point A (t=1.6 s, T=851 K) is just after the T_{max} of the cool flame and point B (t=1.64 s, T=916 K) is just prior to the full ignition. Here we analyse the rate of production of influential species and the highest ranked heat releasing and consuming reactions.

The rate of production analysis of influential intermediate species at points A and B is expressed in Table 1 as percent contributions to the overall rate. The greatest source of hydrogen peroxide is the quadratic interaction of HO_2 radicals. This is supplemented by H atom abstraction by HO_2 from CH_3CHO and CH_2O. At these temperatures decomposition of the acetyl radical dominates its subsequent reactions, thereby generating CH_3 radicals as pre-cursors to formaldehyde. In fact, the most important channel to CH_2O formation is by CH_3O decomposition with C_2H_3 oxidation and $C_3H_7CO_3H$ decomposition also making significant contributions. The major routes to HO_2 formation are by formyl and ethyl radical oxidations. Formyl radicals are formed virtually exclusively from formaldehyde, and they yield HO_2 by oxidation. The importance of formaldehyde and its derivatives in reactions leading to hydrogen peroxide shows that it is a key intermediate in the combustion of n-butane leading to two-stage ignition. This has been shown previously for propane [16].

The ten main exothermic and endothermic reactions at points A and B are shown in Tables 2 and 3 respectively. The sum of the heat release of the 20 reactions at point A is over 70% of the total heat release. As with the rate of production analysis, formaldehyde and its derivatives play a very important role in the heat released by the reaction. This vindicates the conclusion that it is equally instrumental in the development of two-stage ignition as well as the formation of hydrogen peroxide.

A supplementary point connected with the development of two-stage ignition relates to the reactions in which OH radicals are consumed, and especially with regard to the reaction

$$C_4H_{10} + OH \rightarrow C_4H_9 + H_2O. \quad (6)$$

In their paper on the reduced scheme modelling of n-heptane combustion, Peters *et al* [17] claimed that the onset of the second stage of two-stage ignition occurred when OH radicals can no longer be removed by the primary fuel. This is not so for n-butane combustion. At temperatures higher than that of point B in Fig. 6, where the second stage is already well developed in a mixture containing 1.64% n-butane at 0.2 MPa and 600 K, 8% of the fuel still remains at 970 K, for example, and its removal is dominated by reaction (6). Even by 1110 K, 1% of the primary fuel is left and OH radical abstraction continues to contribute significantly to its consumption. However, as shown in Table 4, still more important is the extent to which removal of OH by the primary fuel continues to contribute throughout the early part of the second stage development.

T / K	Reactions consuming OH	%
920	$CH_2O + OH \leftrightarrow CHO + H_2O$	48.2
	$C_4H_{10} + OH \leftrightarrow H_2O + C_4H_9$	13.8
	$H_2O_2 + OH \leftrightarrow H_2O + HO_2$	8.4
	$CH_3CHO + OH \leftrightarrow CH_3CO + H_2O$	5.5
	$C_4H_8 + OH \leftrightarrow C_4H_7 + H_2O$	4.5
970	$CH_2O + OH \leftrightarrow CHO + H_2O$	47.7
	$C_4H_{10} + OH \leftrightarrow H_2O + C_4H_9$	9.6
	$H_2O_2 + OH \leftrightarrow H_2O + HO_2$	8.4
	$CH_3CHO + OH \leftrightarrow CH_3CO + H_2O$	5.1
	$CO + OH \leftrightarrow CO_2 + H$	5.1
1110	$CH_2O + OH \leftrightarrow CHO + H_2O$	44.5
	$CO + OH \leftrightarrow CO_2 + H$	11.3
	$HO_2 + OH \leftrightarrow H_2O + O_2$	7.7
	$OH + H_2 \leftrightarrow H + H_2O$	7.0
	$OH + C_2H_4 \leftrightarrow C_2H_3 + H_2O$	5.3
	$C_4H_{10} + OH \leftrightarrow H_2O + C_4H_9$	2.2

Table 4: Consumption reactions involving OH radicals.

At temperatures well beyond 900 K, reaction (6) remains the second most important route for OH removal and even at 1110 K there is still a 2% contribution to this propagation. Meanwhile, the reaction that dominates the OH radical propagation is the H atom abstraction from formaldehyde

$$CH_2O + OH \rightarrow CHO + H_2O \quad (7)$$

which, of course, feeds into the formation of hydrogen peroxide and its subsequent decomposition, as discussed above. The link of the onset of the second stage to primary fuel depletion seems not to be substantiated in the present case.

Conclusions

Two kinetic schemes have been used to simulate ignition of lean mixtures of n-C_4H_{10} in air. The kinetic schemes have different strengths and weaknesses but there seems to be a common difficulty for reproducing the ignition boundary for $\varphi < 0.6$. The most important reactions leading to hydrogen peroxide involve CH_2O, CHO, HO_2, CH_3CHO and (by implication) CH_3 and CH_3O. Principal routes to heat release in the transition "plateau" region involve the molecular intermediates kinetically linked to formaldehyde and hydrogen peroxide rather than primary fuel. The heat release and kinetic results for n-C_4H_{10} in air presented in this paper are consistent with previously reported C_3H_8 data.

Acknowledgement

The authors gratefully acknowledge financial support from the EU (EVG1-CT-2002-00072-SAFEKINEX)and from EPSRC (GR/ R42726).

References

[1] M.R. Chandraratna, J.F. Griffiths, Combust. Flame 99 (1994) 626.
[2] C.K. Westbrook, Proc. Comb. Inst. 28 (2000) 1563.
[3] M.P. Halstead, A. Prothero, C.P. Quinn, Combust. Flame 20 (1973) 211.
[4] S.W. Benson, Prog. Energy Combust. Sci. 7 (1981) 125.
[5] C. Gibson, J.F. Griffiths. P. Gray, S.M. Hasko, Proc. Comb. Inst. 20 (1984) 101.
[6] J.F. Griffiths, Adv. in. Chem. Phys. 64 (1986) 203.
[7] J.F. Griffiths, B.J. Whitaker, Combust. Flame 131 (2002) 386.
[8] F. Battin-Leclerc, www.ensic.u-nancy.fr/DCPR/ Anglais /GCR/softwares.htm.
[9] V. Warth, F. Battin-Leclerc, R. Fournet, P.A. Glaude, G.M. Côme, G. Scacchi, Comput. Chem. 24 (2000) 541.
[10] C.K. Westbrook, www-cms.llns.gov/combustion /combustion_home.html.
[11] M. Berzins, R.M. Furzland, Shell Research Ltd., TNER 85058, 1985.
[12] T. Turanyi, New J. Chem. 14 (1990) 795.
[13] T. Turanyi, www.chem.leeds.ac.uk/Combustion /kinalc.htm.
[14] T. Turanyi, Reliability Engineering and System Safety 57 (1997) 41.
[15] J.F. Griffiths, K.J. Hughes, M. Schreiber., C. Poppe, Combust. Flame 99 (1994) 533.
[16] J.F. Griffiths, K.J. Hughes, R. Porter, Proc. Comb. Inst. 30 (2004) 1083.
[17] N. Peters, G. Paczko, R. Seiser, K. Seshadri, Combust. Flame 128 (2002) 38.